Acta Scientiarum
http://periodicos.uem.br/ojs
ISSN on-line: 1807-8664
Doi: 10.4025/actascitechnol.v46i1.64413

Comparison between CFD simulation and affinity laws and analysis of the degree of reaction.

Henrique Marcio Pereira Rosa[1*], Rogério Fernandes Brito[2], Álvaro Messias Bigonha Tibiriça[1], Julio Cesar Costa Campos[1] and Felipe Moreton Chohfi[3]

[1]Departamento de Engenharia de Produção e Mecânica, Universidade Federal de Viçosa, Av. PH Rolfs, s/n, 36570-900, Viçosa, Minas Gerais, Brazil. [2]Universidade Federal de Itajubá, Campus Avançado de Itabira, Itabira, Minas Gerais, Brasil. [3]Universidade Federal de Itajubá, Itajubá, Minas Gerais, Brasil. *Autor for correspondente. E-mail: henrique.rosa@ufv.br

ABSTRACT. Computational Fluid Dynamics (CFD) is a modern technology used to study fluid flow. Experimental methods for predicting the turbomachinery performance involve greater time consumption and financial resources compared to the CFD approach. For the centrifugal pump the impeller is the main component, as it transfers energy to the fluid. The pump flow rate and the total head are directly associated with the impeller rotation speed. The purpose of this paper is to present the analysis and comparison of numerical simulation results using Computational Fluid Dynamics of a centrifugal pump impeller under three different rotation speeds: 3500 rpm (nominal), 3100 rpm and 2700 rpm. The software used was ANSYS-CFX®, the turbulence model adopted was the Shear Stress Transport (SST). Eight operating points were simulated for each rotation. The simulation provided the characteristic curves, pressure distribution, and total and static pressure at the inlet and the outlet of the impeller. The degree of reaction was calculated. The results were compared by application of affinity laws, and showed agreement with them. The results also showed that the degree of reaction increased with increasing flow rate, and it was coherent with the backward curved blade impeller. The simulations show that the energy portions that make up the total energy transferred by the impeller agree with the affinity laws.

Keywords: centrifugal pump impeller; numerical simulation; variable rotation; pressure.

Received on July 19, 2022.
Accepted on March 23 2023.

Introduction

Computational fluid dynamics (CFD) is the most current technology in the study of fluid flow used in many applications (Sathish & Mohanavel, 2018; Wehinger, 2019; Zhang & Mirzael, 2020; Chavan, Vitankar, Shinde, & Thorat, 2021). Experimental methods of turbomachinery performance prediction involve greater consumption of time and financial resources compared to the CFD approach, which has been widely used in fluid flow simulation in turbomachinery (Abdelmadjid, Mohamed, & Boussad, 2013; Danish, Khan, Umer, Qureshi, & Ma, 2014; Liu, Wang, Wang, Huang, & Jiang, 2014; Nataraj & Singh, 2014). Successful results in predicting flow patterns in centrifugal pumps indicate that CFD may be able to assist a pump engineer in achieving improved designs (Yedidiah, 2008). Many researchers have applied the CFD tool in the study of pumps and turbomachinery in general.

Shojaeefard, Tahani, Ehghaghi, Fallahian, and Beglari (2012) used CFD to evaluate the influence of blade angle and width at the impeller exit of a centrifugal pump on the flow behavior for two different fluids: water and oil. Some combinations of three blade angle (27.5, 30 and 32.5°) and two widths (17 and 21 mm) were studied. It was found that there was a variation on pump head and efficiency, and that 30° angle with 21mm width was the best combination.

Zhu, Li, Jiang, and Fu (2016) investigated the influence of diffuser blade height on the performance of a centrifugal pump with a 6-bladed impeller and low specific speed. The pump performance was evaluated when the diffuser blade height was 0 (no blade), 0.5, 0.6, 0.8, and 1 time the diffuser width.

Xiaoran et al. (2018) employed the CFD tool to analyze the asymmetric flow characteristics in a reversible turbine pump operating in pump mode, taking the relationship between pressure fluctuations and unsteady flow pattern in the impeller as the premise of analysis. Wang, Wang, Kong, Gou, and Yang (2017) proposed changes in the blade profile of a pump impeller so that it could operate as a turbine with good performance.

In this study, the hydraulic loss, internal flow characteristic, and static pressure distribution were analyzed based on the numerical results obtained by CFD.

Rosa and Emerick (2020) evaluated the influence of intermediate blades inserted between the main blades in a centrifugal pump impeller. The intermediate blades were 30% longer as compared to the main blade. CFD results of three configurations were compared as follows: 1) without intermediate blade; 2) with intermediate blades at the inlet; 3) with intermediate blades at the outlet.

Lorusso et al. (2017) developed a procedure with general rules to be applied when creating meshes suitable for CFD simulation to study cavitation in centrifugal pumps. Concerning cavitation, Jaiswal, Rehman, Paul, and Jain (2019) used CFD applied on centrifugal pump impeller to determine the sound pressure at a particular value of net positive suction head (NPSH) corresponding to incipient cavitation and super-cavitation. In this study the vapor volume fraction and the drop in head in the impeller were also computed with the input power and output power required for the pump.

A useful feature of CFD is that it provides information that is impossible to obtain through experimental procedures. At any point or region of the flow field one can obtain pressure and velocity values and also visualize the distribution of these parameters in the regions. Thus, CFD is a useful analysis. The CFD simulation results made possible the detailed study of principles and laws governing the behavior of fluid systems. One possible analysis is the application of the affinity laws of turbomachinery for different rotations. These laws are not deduced from three-dimensional transport equations solved by the CFD solver. They are obtained from dimensionless parameters like flow and pressure coefficients, which come from an analysis method based on the similarity between flows.

For centrifugal pumps the impeller is the main component because it is responsible for transferring energy to the fluid. The pump flow rate and the total head are directly associated with the impeller rotation speed. In this context, this work presents a comparative study between CFD simulation and the application of the affinity laws for a centrifugal pump impeller under three different rotations. The characteristic curves ($H_{impeller}$xQ) and the pressure distribution in a transverse plane passing through the midpoint of the impeller exit width were analyzed. The behavior of the reaction degree as a function of flow rate for three different rotations was also studied. This allowed verifying if the portions that compose the total energy supplied by the impeller also agree with the affinity laws.

Material and methods

In this work a centrifugal pump impeller with 6 backward curved blades, nominal flow rate 40 m^3/h and rotation 3500 rpm were analyzed. Table 1 below presents the geometric data.

Table 1. Geometric parameters of the impeller.

D_1	D_2	B_t	B_2	β_1	β_2	z
(mm)				(°)		-
54.9	149.0	4.5	10.9	29.0	25.0	6

Where:

D_1 – Inlet diameter;
D_2 – Outlet diameter;
B_t – Blade thickness;
B_2 – Output width;
β_1 – Blade angle at the entrance;
β_2 – Blade angle at exit;
z – Number of blades.

Computational simulation

The CFD simulation tool uses numerical methods to calculate the pressure and velocity parameters of the 3-D flow field. This work used the commercial software Ansys-CFX® to study the flow domain presented in Figure 1.

Mesh construction

To perform the calculations, it is necessary to discretize the domain into small elements (mesh). In this work, an unstructured mesh with mostly tetrahedral elements was made using the meshing software, which

is part of the Ansys package. Refinements near the edges were necessary, as it is a region of interest due to the occurrence of important physical phenomena. In areas with high curvature or near the surface the "sizing" function-controlled growth and mesh distribution. The inflation function was applied to the elements adjacent to the blade surface. Figure 2 shows the constructed mesh.

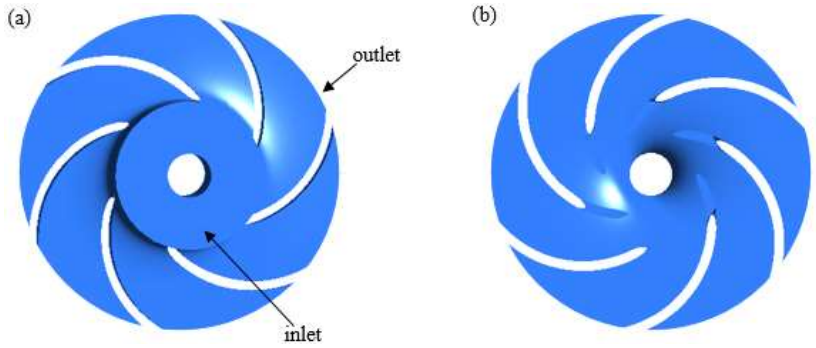

Figure 1. Fluid domain; (a) front view, and (a) rear view.

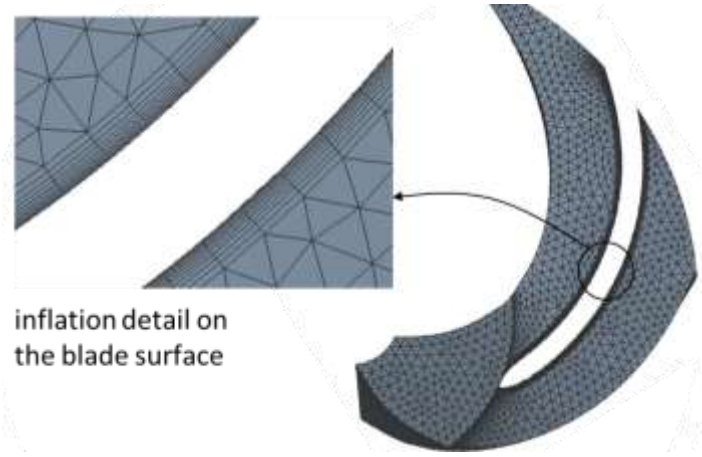

Figure 2. Mesh.

Due to symmetry condition and in order to work on a more refined and better-quality mesh without consuming too much computational memory a mesh was built in the flow channel that involves only one blade. In Ansys-CFX® software this condition is commonly chosen and indicated for geometries that have symmetries.

Mesh refinement has a limit beyond which further refinement will not yield accurate results. The search for this limit is the mesh test, which consists in evaluating the variation of a reference parameter as a function of the mesh size. A variation of less than 0.5% is a value adopted as satisfactory (Yang, Derakhshan, & Kong, 2012; Derakhshan, Pourmahdavi, Abdolahnejad, Reihani, & Ojachi, 2013).

Figure 3 shows the graph of the mesh test. The final mesh used in the simulations has 276,795 elements.

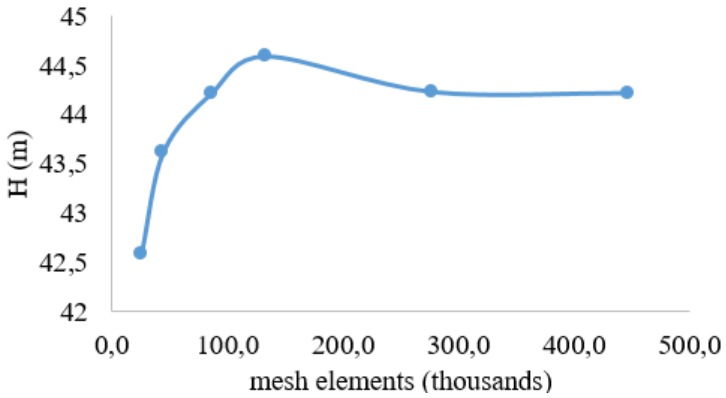

Figure 3. Mesh test.

Boundary conditions and simulation methodology

In addition to the mesh, the boundary conditions to be applied to the fluid domain must be defined. Figure 1A shows the inlet and outlet regions. At the inlet the mass flow rate value was assigned and at the outlet, the static pressure. In the other regions, there is no flow through, so they were set up as walls. The condition of smooth and non-slip walls was adopted (Ansys, 2010).

Changing the mass flow rate value allowed to simulate several operation points. Simulations were performed for three rotation speeds: nominal, 3100 and 2700 rpm, in clockwise sense. The static pressures at the outlet were constant for all points of the same rotation, but different between rotations: 295, 230 and 175 kPa respectively.

Three sets of simulations were performed, each referring to one rotation. Each set consisted of 8 operating points. For the nominal speed rotation, the simulated flow rates were defined as percentages of the nominal flow rate. For the other speeds, the flow rates were those of the points homologous to the nominal speed points.

The reference pressure was 101.325 kPa and the fluid properties were those of water at 25°C.

The turbulence model used was the SST (Shear Stress Transport). This model is very accurate for numerical investigations of flow in centrifugal pumps (Shojaeefard et al., 2012; Zhu, Li, Jiang, & Fu, 2016; Lorusso et al., 2017; Jaiswal, Rehman, Paul, & Jain, 2019). SST was developed by Menter (1994) and is a hybrid model that combines features of κ–ε and κ–ω. The κ–ε algorithm provides results more accurate in regions of flow far from walls. On the other hand, κ–ω better computes near-wall phenomena. The SST model combines the two through an automatic function for treating near-wall flow. Using the dimensionless distance from the wall as a comparison parameter, the automatic function selects which algorithm to use, so that in regions close to walls, the κ–ω is used, and in distant regions, the κ–ε

For solving the advective term, the "high-resolution" method was set up. The convergence criterion was an RMS residual less than 10^{-4}.

Head supplied by the impeller

The total energy transferred by the impeller to the fluid is in the form of static and dynamic pressure energy that is total pressure (Stepanoff, 1957; Sedille, 1967; Turton, 1995).

Equation 1 give the energy transferred by the impeller to the fluid in terms of head.

$$H_{impeller} = \frac{\Delta P_{Total}}{\rho g} \quad (1)$$

Where:

$H_{impeller}$ - Head supplied by the impeller to the fluid, in m;

ΔP_{Total} - Total pressure gain (static + dynamic) between inlet and outlet, in Pa;

ρ - Density of water, kg m^{-3};

g - Acceleration of gravity, in m s^{-2}.

The specific density of water being 997 kg m^{-3} (at 25ºC), and the acceleration of gravity 9.80665 m s^{-2}.

The total pressure values at the inlet and outlet sections are averages weighted by the mass flow rate at the respective sections.

Variable rotation speed

Although the hydraulic and mechanical design of a centrifugal pump are associated with a constant rotation speed, the variation of rotation is a method used to adjust the operation of the pump to the demands of the system, which in some cases suffer large variations over time. The use of this technology makes it possible to maintain pressures and flows close to the minimum levels allowed, which represents a potential energy saving (Wu, Simpson, Maier, & Marchi, 2012). According to Kalaiselvan, Subramaniam, Shanmugam, and Hanigovszki (2016) this is the main method to improve energy efficiency in pumping systems, and has been the subject of study by several researchers, such as: Ahonen et al. (2010), Tamminen et al. (2013), Coutinho and Soares (2017).

The values of flow rate and head at different rotations are calculated by applying the affinity laws (Equations 2 and 3) for homologous points.

$$\frac{Q_1}{Q_2} = \frac{N_1}{N_2} \quad (2)$$

$$\frac{H_{impeller\ (1)}}{H_{impeller\ (2)}} = \left(\frac{N_1}{N_2}\right)^2 \quad (3)$$

Where:
Q - Flow rate;
N – Rotation speed;
1 and 2 - indicates two distinct rotations speed

Results and discussion

Figure 4 presents the characteristic curves of the head delivered by the impeller (Eq. (1)) per flow rate for the three rotations, obtained from simulation results.

The downward behavior of the curves is consistent with centrifugal pump impeller curves.

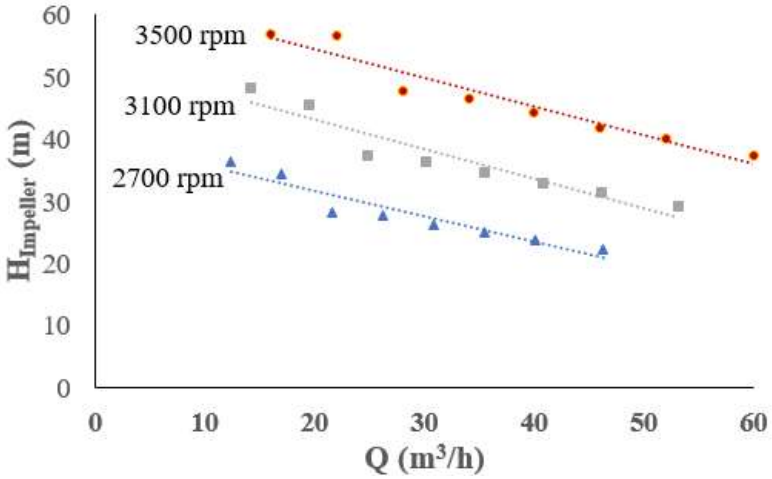

Figure 4. Characteristic curves for the 3 rotations.

Another way to obtain the impeller head, besides simulation, is by applying the affinity law (Eq. (3)) to the values for the 3500 rpm speed for the speeds of 3100 and 2700 rpm. Thus, it is possible to compare the values obtained from the simulations with those obtained by applying the affinity laws. Table 2 presents both values for the homologous points.

Table 2 shows that for points 3 to 8 the head obtained from simulations and from the affinity laws were practically the same, with relative errors lower than 0.05%, indicating a high degree of agreement of the numerical simulation with the affinity laws.

For points 1 and 2, the differences were greater, close to 7.5% for the first point, and 2.5% for the second point. These points are those of lower flow rate, respectively 40 and 55% of the nominal flow rate. The largest error was for the lowest flow rate. These values suggest three possibilities of analysis for flow rate much lower than the nominal: 1) the affinity law does not adjust perfectly; 2) the CFD simulation does not capture correctly the occurring phenomena; or 3) a combination of the first two. With the available elements, it is not possible to say which of the three is the most probable.

Table 2. Head supplied by the impeller for homologous points.

		3100 rpm			2700 rpm		
Homologous point	% Qn	H Afinity (m)	H CFD (m)	Relative error (%)	H Afinity (m)	H CFD (m)	Relative error (%)
1	40%	44.72	48.14	7.6476	33.93	36.46	7.4565
2	55%	44.44	45.49	2.3627	33.71	34.52	2.4028
3	70%	37.37	37.36	0.0268	28.35	28.34	0.0353
4	85%	36.47	36.47	0.0000	27.67	27.66	0.0361
5	100%	34.69	34.69	0.0000	26.32	26.32	0.0000
6	115%	32.85	32.85	0.0000	24.92	24.92	0.0000
7	130%	31.42	31.43	0.0318	23.84	23.84	0.0000
8	150%	29.33	29.34	0.0341	22.25	22.26	0.0449

Pressure distribution analysis

Figure 5 shows the static pressure distribution in a transverse plane passing through the midpoint of the width at the impeller outlet for the nominal flow rate for each speed.

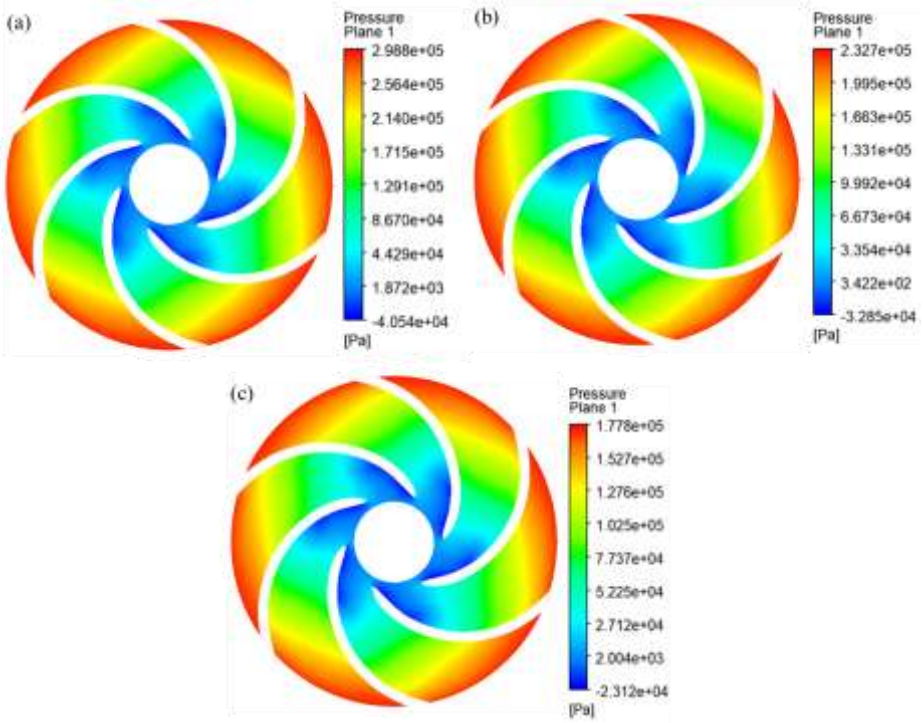

Figure 5. Static pressure distribution; (a) 3500 rpm; (b) 3100 rpm; and (c) 2700 rpm.

The figure shows that the pressure contour is the same for the three speeds with only one change in the minimum pressure values: the maximum pressure decreases with decreasing speed, and the minimum pressure increases.

The pressure distribution indicates the following elements:

1) the static pressure increases gradually with the radius of the impeller;
2) for the same radius, the pressure on the front face of the blade is higher than on the rear face;
3) near the exit edge of the blades the pressures of the two faces tend to equalize;
4) the static pressure in the inlet region of the blades is low, being negative in some places.

These elements reveal a behavior consistent with the turbomachinery theory (Stepanoff, 1957; Sedille, 1967).

Analysis of the degree of reaction

The degree of reaction of a centrifugal pump impeller indicates how much of the total energy delivered by the impeller to the fluid is in the form of static pressure energy. This is an important parameter in impeller analysis because the primary utility of a centrifugal pump is the production of hydraulic energy in the form of static pressure. Equation (4) gives the degree of reaction (Turton, 1995).

$$R = \frac{\Delta P_{Est}}{\Delta P_{Total}} \quad (4)$$

Where:

R - degree of reaction;

ΔP_{Est} - Static pressure gain between inlet and outlet, in Pa.

The CFD simulation provides the averaged values of the static and total pressure at impeller inlet and outlet. With these values it is possible to calculate the static and total pressure gains, the dynamic pressure gain (difference between the total and static pressure) and the degree of reaction (Equation 4). Table 3 presents these results.

The values of the static and total pressures, used to calculate the gains, are weighted averages in the respective sections, with their static pressure weighted by area and the total pressure weighted by mass flow.

Table 3. Pressure gains and degree of reaction.

	% Qn	Pressure Gains (kPa)			Degree of reaction
	----	Static	total	dynamic	----
3500 rpm	40%	309.509	557.583	248.074	0.555
	55%	302.323	554.011	251.688	0.546
	70%	297.209	465.928	168.719	0.638
	85%	298.255	454.731	156.476	0.656
	100%	294.989	432.554	137.565	0.682
	115%	289.697	409.499	119.802	0.707
	130%	284.956	391.768	106.812	0.727
	150%	275.587	365.727	90.140	0.754
3100 rpm	40%	244.047	470.668	226.621	0.519
	55%	237.530	444.762	207.232	0.534
	70%	233.091	365.308	132.217	0.638
	85%	233.935	356.579	122.644	0.656
	100%	231.196	339.133	107.937	0.682
	115%	227.060	321.206	94.146	0.707
	130%	223.388	307.316	83.928	0.727
	150%	216.060	286.872	70.812	0.753
2700 rpm	40%	185.130	356.475	171.345	0.519
	55%	180.172	337.530	157.358	0.534
	70%	176.737	277.118	100.381	0.638
	85%	177.425	270.415	92.90	0.656
	100%	175.280	257.301	82.021	0.681
	115%	172.029	243.603	71.574	0.706
	130%	169.316	233.112	63.796	0.726
	150%	163.786	217.604	53.818	0.753

The analysis of the table shows that:

1) the degree of reaction is practically the same for the homologous points, with differences of less than 0.01%. In the case of the lower flow rate points, 40 and 55% Qn, the results show respectively, 6.6 and 2.1%. These results indicate that the affinity laws can be applied to the portions (static and dynamic) that make up the total energy delivered by the impeller;

2) for all flow rates the static pressure gain is always greater than the dynamic one, which results in a degree of reaction greater than 0.5. This was expected, because according to the turbomachinery theory, an impeller with backward curved blades should present a degree of reaction greater than 0.5. (Stepanoff, 1957);

3) the degree of reaction increased with increasing flow rate, going from values close to 0.53 for the lowest flow rate to 0.75 for the highest. This indicates that the proportion of dynamic energy decreased at higher flow rates. Calculating the ratio between the dynamic and static pressure gain, the ratio for the 3500 rpm rotation is 0.80 for the lowest flow rate, and 0.33 for the highest. For the 3100 and 2700 speeds, they are 0.92 and 0.33. These numbers show a larger dynamic pressure gain compared to static pressure gain;

4) it seems contradictory that the dynamic energy decreases with the flow increase, however, this occurs because the dynamic energy is obtained using the absolute velocities at the entrance and exit of the impeller blades. For smaller flow rates these velocities increase, the opposite occurs for larger flow rates (Stepanoff, 1957; Sedille, 1967; Turton, 1995).

Conclusion

According to the results presented, it is concluded that:

- The values of the total energy supplied by the impeller obtained with the CFD simulation for rotational speeds different from the nominal were equal to those obtained by applying the affinity laws, except for the points of lower flow: 40 and 55%, although for these the differences were small, 6,6 and 2,1% respectively, and are within an error margin acceptable;
- The values of the degree of reaction also agreed with the affinity laws. This shows that the affinity laws can also be applied to the static and dynamic pressure energy portions;

- For the three rotations, the static and dynamic pressure gains decreased with the flow rate. However, for the dynamic pressure the variations were greater. Consequently, the degree of reaction increased with the increase of the flow rate;
- The static pressure distribution in the transverse plane passing through the midpoint of the impeller exit width was found to be consistent with turbomachinery theory for three rotations;
- This work indicates that the use of affinity laws to validate CFD simulations in turbomachines is a possibility that should be studied and tested in other cases.

Acknowledgment

The authors thank the funding agencies in the Brazil: The National Research Council (CNPq) and the Foundation for Supporting Research in the state of Minas Gerais (FAPEMIG).

References

Abdelmadjid, C., S. Mohamed, & Boussad, B. (2013). CFD Analysis of the Volute Geometry Effect on the Turbulent Air Flow through the Turbocharger Compressor. *Energy Procedia*, *36*, 746-755. DOI: https://doi.org/10.1016/j.egypro.2013.07.087

Ahonen. T., J. Tamminen, J. Ahola, J. Viholainen, N. Aranto, & Kestila, J. (2010). Estimation of Pump Operational State with Model-Based Methods. *Energy Conversion and Management*, *51*(6), 1319-1325. DOI: https://doi.org/10.1016/j.enconman.2010.01.009

Ansys Inc. (2010). *Ansys CFX Tutorials* (p. 636). Canonsburg, PA: SAS IP Inc.

Chavan, A., Vitankar, V., Shinde, N., & Thorat, B. (2021). CFD Simulation of Solar Grain Dryer. *Drying Technology*, *39*(8), 1101-1113. DOI: https://doi.org/10.1080/07373937.2020.1863422

Coutinho, R. S., & Soares, A. K. (2017). Simulation of Pumps with Variable Rotation Speed in EPANET. *Sanitary and Environmental Engineering, 22*(4), 797-808. DOI: https://doi.org/10.1590/S1413-41522017163428

Danish, S. N., Khan, S. D. D., Umer, U., Qureshi, S. R., & Ma, C. (2014). Performance Evaluation of Tandem Bladed Centrifugal Compressor. *Engineering Applications of Computational Fluid Mechanics*, *8*(3), 382-395. DOI: https://doi.org/10.1080/19942060.2014.11015523

Derakhshan, S., M. Pourmahdavi, E. Abdolahnejad, A. Reihani, & Ojachi, A. (2013). Numerical Shape Optimization of a Centrifugal Pump Impeller using artificial bee colony algorithm. *Computers and Fluids*, *81*, 145-151. DOI: https://doi.org/10.1016/j.compfluid.2013.04.018

Jaiswal, A. K., Rehman, A. U., Paul, A. R., & Jain, A. (2019). Detection of Cavitation through Acoustic Generation in Centrifugal Pump Impeller. *Journal of Applied Fluid Mechanics*, *12*(4), 1103-1113. DOI: https://doi.org/10.29252/jafm.12.04.29501

Kalaiselvan, A. S. V., Subramaniam, U., Shanmugam, P., & Hanigovszki, N. (2016). A Comprehensive Review on Energy Efficiency Enhancement Initiatives in Centrifugal Pumping System. *Applied Energy*, *181*(5), 495-513. DOI: https://doi.org/10.1016/j.apenergy.2016.08.070

Liu, H., Wang, J., Wang, Y., Huang, H., & Jiang, L. (2014). Partially-Averaged Navier-Stokes Model for Predicting Cavitating Flow in Centrifugal Pump. *Engineering Applications of Computational Fluid Mechanics*, *8*(2), 319-329. DOI: https://doi.org/10.1080/19942060.2014.11015517

Lorusso, M., Capurso, T., Torresi, M., Fortunato, B., Fornarelli, F., Camporeale, S. M., & Monteriso, R. (2017). Efficient CFD Evaluation of the NPSH for Centrifugal Pumps. *Energy Procedia*, *126*, 778-785. DOI: https://doi.org/10.1016/j.egypro.2017.08.262

Menter, F. R. (1994). Two-Equation Eddy-Viscosity Turbulence Models for Engineering Applications. *AIAA-Journal*, *32*(8), 1598-1605.

Nataraj, M., & Singh, R. R. (2014). Analyzing Pump Impeller for Performance Evaluation using RSM and CFD. *Desalination and Water Treatment*, *52*(34-36), 6822-6831. DOI: https://doi.org/10.1080/19443994.2013.818924

Rosa, H. M. P., & Emerick, B. S. (2020). CFD Simulation on Centrifugal Pump Impeller with Splitter Blades. *Revista Brasileira de Engenharia Agrícola e Ambiental*, *24*, 3-7. DOI: https://doi.org/10.1590/1807-1929/agriambi.v24n1p3-7

Sathish, T., & Mohanavel, V. (2018). IWF based Optimization of Porous Insert Configurations for Heat Transfer Enhancement using CFD. *Journal of Applied Fluid Mechanics*, *11*, 31-37. DOI: https://doi.org/10.36884/JAFM.11.SI.29414

Sedille, M. (1967). *Turbomachines Hydrauliques et Thermiques.* Tome 2. Paris: Masson and Cie Éditeurs.

Shojaeefard, M. H., Tahani, M., Ehghaghi, M. B., Fallahian, M. A., & Beglari, M. (2012). Numerical Study of the Effects of some Geometric Characteristics of a Centrifugal Pump Impeller that umps a Viscous Fluid. *Computers & Fluids*, *60*, 61-70. DOI: https://doi.org/10.1016/j.compfluid.2012.02.028

Stepanoff, A. J. (1957). *Centrifugal and Axial Flow Pumps: Theory, Design and Applications* (2nd ed.). New York, NY: John Wiley and Sons Inc.

Tamminen, J., Viholainen, J., Ahonen, T., Ahola, J., Hammo, S., & Vakkilainen, E. (2013). Comparison of Model-Based Flow Rate Estimation Methods in Frequency-Converter-Driven Pumps and Funs. *Energy Efficiency*, *7*, 493-505. DOI: https://doi.org/10.1007/s12053-013-9234-6

Turton, R. K. (1995). *Principles of Turbomachinery*, (2nd ed.). London, EUA: Chapman and Hall.

Wang, T., Wang, C., Kong, F., Gou, Q., & Yang, S. (2017). Theoretical, Experimental, and Numerical Study of Special Impeller used in Turbine Mode of Centrifugal Pump as Turbine. *Energy*, *130*, 473-485. DOI: https://doi.org/10.1016/j.energy.2017.04.156

Wehinger, G. D. (2019). Radiation Matters in Fixed-Bed CFD Simulations. *Chemie Ingenieur Technik*, *91*(5), 583-591. DOI: https://doi.org/10.1002/cite.201800179

Wu, W., Simpson, A., Maier, H., & Marchi, A. (2012). Incorporation of Variable-Speed Pumping in Multiobjective in Genetic Algorithm Optimization of the Design of Water Transmission Systems. *Water Resources Planning and Management, 138*(5), 543-552. DOI: https://doi.org/10.1061/(ASCE)WR.1943-5452.0000195

Xiaoran, Z., Yexiang, X., Zhengwei, W., Hongying, L., Soo-Hwang, A., Yangyang, Y., & Honggang, F. (2018). Numerical Analysis of Non-Axisymmetric Flow Characteristic for a Pump-Turbine Impeller at Pump Off-Design Condition. *Renewable Energy*, *115*, 1075-1085. DOI: https://doi.org/10.1016/j.renene.2017.06.088

Yang, S. S., Derakhshan, S., & Kong, F. Y. (2012). Theoretical, Numerical and Experimental Prediction of Pump as Turbine Performance. *Renewable Energy*, *48*, 507-513. DOI: https://doi.org/10.1016/j.renene.2012.06.002

Yedidiah, S. (2008). A Study in the Use of CFD in the Design of Centrifugal Pumps. *Engineering Applications of Computational Fluid Mechanics*, *2*(3), 331-343. DOI: https://doi.org/10.1080/19942060.2008.11015233

Zhang, R. J., & Mirzael, P. A. (2020). CFD-CFD Coupling: A Novel Method to Develop a Fast Urban Microclimate Model. *Journal of Building Physics*, *44*(5), 385-408. DOI: https://doi.org/10.1177/1744259120935921

Zhu, X., Li, G., Jiang, W., & Fu, L. (2016). Experimental and numerical investigation on application of half vane diffusers for centrifugal pump. *International Communications in Heat and Mass Transfer, 79*, 114-127. DOI: https://doi.org/10.1016/j.icheatmasstransfer.2016.10.015